Research paper

Transforming diatomaceous earth into sensing devices by surface modification with gold nanoparticles

M. Villani [a], V. Onesto [b], M.L. Coluccio [b], I. Valpapuram [b], R. Majewska [c,d], A. Alabastri [e], E. Battista [f], A. Schirato [g], D. Calestani [a], N. Coppedé [a], A. Zappettini [a], F. Amato [b], E. Di Fabrizio [h], F. Gentile [i,*]

[a] IMEM-CNR, Parco Area delle Scienze 37/A, 43124 Parma, Italy
[b] Department of Experimental and Clinical Medicine, University Magna Graecia, 88100 Catanzaro, Italy
[c] Unit for Environmental Sciences and Management, School of Biological Sciences, North-West University, 2520 Potchefstroom, South Africa
[d] South African Institute for Aquatic Biodiversity, Grahamstown 6140, South Africa
[e] Department of Physics and Astronomy, Rice University, 77005 Houston, TX, USA
[f] Interdisciplinary Research Center on Biomaterials, University Federico II, 80125 Naples, Italy
[g] Department of Physics, Politecnico di Milano, I-20133 Milan, Italy
[h] King Abdullah University of Science and Technology, Thuwal 23955-6900, Saudi Arabia
[i] Department of Electrical Engineering and Information Technology, University Federico II, 80125 Naples, Italy

ARTICLE INFO

ABSTRACT

Diatomaceous earth, or diatomite, is produced through the accumulation of diatom (Bacillariophyceae) skeletons (i.e. cell walls called frustules) made of amorphous silica. The porous, highly symmetrical structure and microscopic size of diatom cell walls make them ideal constituents of sensing devices and analytical chips. Here, we propose chemical methods to purify diatom frustules extracted from diatomaceous earth. Using photo deposition techniques, we grow gold nanoparticles on the surface of diatom skeletons and within the pores of the skeletons, where the size and density of nanoparticles can be controlled by changing the parameters of the synthesis. Resulting devices have an internal porous structure that can harvest molecules from a solution, and an external shell of gold nanoparticles that amplifies the electromagnetic field generated by the measurement laser in Raman or other spectroscopies. The combination of these effects enables the analysis of biological specimens, chemical analytes and pollutants in extremely low abundance ranges. The devices were demonstrated in the analysis of Bovine Serum Albumin in water with a concentration of 100 aM, and mineral oil with a concentration of 50 ppm.

1. Introduction

Diatomaceous earth is a natural, theoretically non-depletable material composed of fossilized diatom shells (silicon dioxide) with intricate and highly symmetrical patterns of pores and more complex openings penetrating through their surface [1,2]. The arrangement, shape, and size of the openings, which vary in various species and in different sections of the diatom cell wall ranging from few tens of nanometers to few micrometers, impart to the shells' mechanical [3] and optical properties [4–7] that are more frequently found in artificial micro and nano devices. Due to their unique characteristics, diatom shells show promise to be used as low cost, highly efficient drug carriers, sensor devices or other devices for biological and safety applications. However, to date there are relatively few applications of diatom integrated devices in biomedicine.

Current approaches for diatom treatment and functionalization necessitate heating diatom shells to high temperatures in a controlled atmosphere of magnesium gas [8,9] to convert silicon dioxide into silicon. While the conversion preserves the original shape of the diatom frustules, silicon can be efficiently used for surface chemical and biochemical treatments. Alternative chemical formulations for changing the surface chemistry and characteristics of diatom shells involve electroless deposition as in references [10, 11], in which case the process requires multiple steps in cascade with some of them as long as ~90 h. Sophisticated, complex, and complicated functionalization techniques may be difficult to implement and can hamper the translation from a prototype to a marketable product.

Here, we demonstrate easy ways for the site-selective functionalization of diatom shells with gold nanoparticles. The method is based on a photo-deposition process. Diatomaceous earth undergoes selective etching to remove unwanted debris and activate the surface of the frustules for the subsequent deposition of gold nanoparticles. The nucleation/growth process is performed by suspending diatom shells in an alcoholic solution of chloroauric acid and exposing them to ultra

violet radiation for a total irradiation time that does not exceed 1 h. The process enables the synthesis of gold nanoparticles on the surface and inside the pores of diatom shells with variable size and density. Subsequently, the performance of the devices as SERS (Surface Enhanced Raman Spectroscopy) devices is assessed by detecting and harvesting bovine serum albumin and mineral oil in low abundance ranges. SERS is an effect whereby the Raman signal in close proximity of a metal nano-structure is enhanced by several orders of magnitude compared to a flat surface without structuration. Owing to the geometry of the metal nanomaterials, electrons on the surface of the material oscillate collectively when excited by an external radiation, in a resonance effect. This generates plasmons, i.e. surface waves, and consequently an amplification of the intensity of the local electromagnetic (EM) field. Since the Raman signal is proportional to the power of four of the EM field, the entire mechanism yields a giant amplification of the Raman readout, enabling high resolution, high sensitivity, and low limits of detection of a measurement. Proposed methods may have implications in analytical chemistry, bioengineering, medicine, the analysis, monitoring and traceability of chemical pollutants and biomolecules.

2. Materials and methods

2.1. Functionalizing diatom frustules with gold nanoparticles

Diatomaceous Earth (DE) was cleaned with piranha solution to remove possible contaminants and organic residuals. Samples were then maintained for 120 s in a diluted 2% hydrofluoric acid (HF) solution to activate the diatom frustule surface and promote Au nucleation. Gold nanoparticles (Au NPs) were then synthetized on the diatom surfaces by a photo-deposition process. 20 mg of diatom shells were suspended in 50 ml of isopropyl alcohol (IPA) and irradiated with a UVA/UVB Osram Ultra Vitalux lamp for 1 h. During irradiation, a 0.1% w/w solution of chloroauric acid in IPA was timely injected to the suspension of DE in IPA in aliquots of 150 μl, every 5 min. Diatom shells functionalized with Au NPs are called D24 systems throughout the current paper. Notice that by varying the irradiation time, the concentration of diatom shells in solution and amount of chloroauric acid, one can obtain a variety of different nanoparticle morphologies. While optimized in the present work, the photo-induced process of nanoparticle growth is not completely new. In previously reported works, some of the authors of this paper have generated branched gold nanoparticles on zinc oxide ZnO tetrapods, where the overall size of the particles is varied between 20 and 40 nm, and the size of the protrusions is controlled in the 5 − 8 nm interval [12,13]. Also notice that the present photo-irradiation method is significantly different from electroless deposition techniques, where gold cations are reduced to metal onto autocatalytic surfaces [14,15].

2.2. SEM characterization of samples

D24 systems were immobilized on a carbon adhesive tape for SEM (Scanning Electron Microscope) imaging. For morphological imaging, samples were imaged using a Zeiss Auriga Compact FE-SEM equipped with InLens secondary-electron detector. An annular back scattering detector was used for Z-contrast imaging and to highlight the presence of Au in the samples.

2.3. Finite element method (FEM) simulation of the EM field around the D24 systems

We used finite element method (FEM) to derive the EM distributions within the samples. Simulations have been conducted on a single cubic unit cell with 125 particles decorating the diatom shell. We represented the diatom as a dielectric with an index of refraction $n = 1.3$. We modelled the Au NPs as perfect spheres with an external diameter $d = 10$ nm and dielectric characteristics as in the classical formulation of Rakic reported in reference [16]. We imposed for the medium surrounding the diatom and the particles the refractive index of air $n = 1.0$. We used tetrahedral mesh elements to discretize the domain. The maximum allowable element size was imposed as 0.2 times the wavelength of the radiation propagating in each region of the domain. The minimum element size was set to $d/3$. Then, we interrogated the systems with a TM linearly polarized plane wave with variable angle of incidence. We used Floquet periodic boundary conditions at the boundaries of the domain to reduce the computation time and increase the efficiency of the simulations. The incident radiation had wavelength $\lambda = 633$ nm, power $P = 1$ W, and intensity $I = 2.5 \times 10^{-8}$ W/cm^2 within an area of the unit cell of $A = 3.9 \times 10^{-13}$ m^2. Maxwell equations have been solved by placing perfectly matched layers at the top and the bottom of the structure, to avoid unphysical reflections at the boundaries of the domain. Equations were solved for a half of a diatom – perfect magnetic conductor boundary conditions have then been imposed to the lateral sides of the unit cell, parallel to the plane of incidence, coherently with the polarization of the incident field.

2.4. Fluorescence analysis of D24 systems

We incubated the D24 systems with Fluoresbrite Yellow Green 50 nm spheres for 10 min using a relative abundance of 1 to 10 (diatoms to fluorescent beads). We then collected the diatom devices and positioned them on the stage of an optical inverted Leica TCS-SP2 laser confocal microscope. We then used an ArUV laser to examine the fluorescence response of the systems. In analyzing the fluorescence, we set constant values of the pinhole aperture (80 μm) and laser power (80% power) throughout the measurements. Yellow fluorescence was induced using a wavelength of $\lambda = 441$ nm and was acquired at the wavelength $\lambda = 485$ nm, corresponding to the maximum of
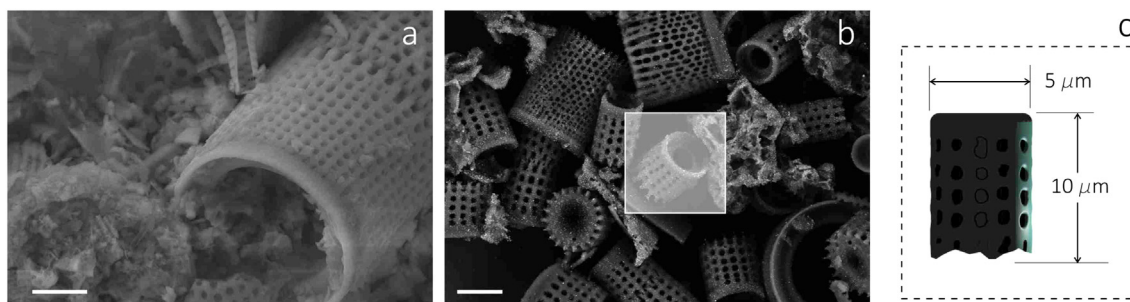

Fig. 1. Pristine diatomaceous earth is a collection of silicon dioxide shells mixed with debris and other organic/inorganic contaminants, scale bar in the image is 2 μm (a). After treatment with *HF*, we obtain a more uniform distributions of shells (scale bar in the image is 10 μm) (b), where each shell is a hollow cylinder with average length at the base of ~5 μm and height ~10 μm (c).
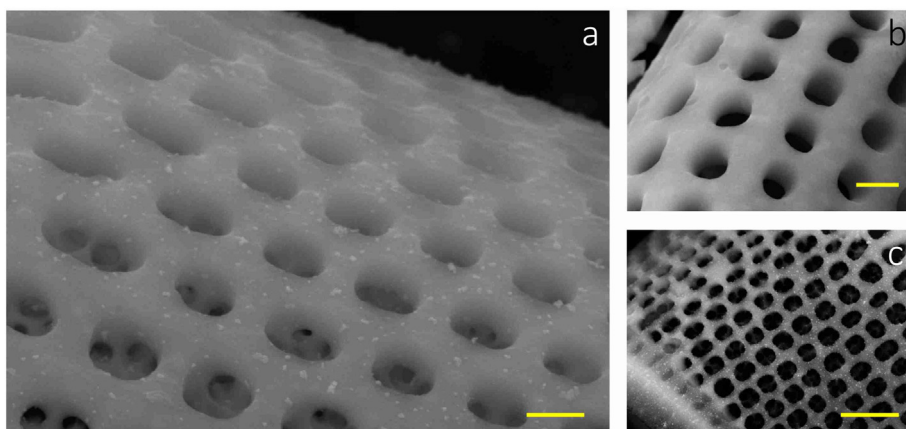
Fig. 2. SEM images of the diatoms indicate that that the average size of the pores penetrating through the shells is ~90 μm with small deviations around the mean, scale bar in the image is 100 nm (a). Additional SEM images show that the arrays of pores on the external diatom surface reproduce an hexagonal pattern as in a photonics crystal (b, c). Scale bar is 150 nm in (b) and 400 nm in (c).

emission of the beads. Images were acquired using 10/20× objectives focusing on a region of interest of 975 × 750 μm^2, and were averaged on 4 lines and 10 frames to reduce noise and improve quality.

2.5. Using the D24 systems as SERS devices for Raman analysis of samples

Upon incubation of D24 devices with Bovine Serum Albumin (BSA) and mineral oil (mo), samples were positioned on the stage of a Renishaw InVia micro-Raman microscope for analysis. Samples were analyzed using 20/50×objectives of a Leica microscope. We used a HeNe laser with a wavelength $\lambda = 633$ nm and backscattering geometry to analyze samples. Laser power was adjusted as $P = 0.18$ mW throughout the measurements. Raman signal was digitalized into 1024 × 1024 pixels of the CCD of a recording camera. Images were recorded with an integration time of 20 s. After acquisition, Raman spectra were base-line corrected with a second degree polynomial function.

3. Results

Diatomaceous earth as received is a non-continuous, non-homogeneous collection of porous, amorphous silica (SiO$_2$) shells, with unwanted biological, organic and inorganic fragments and remains infiltrating between the diatoms (Fig. 1a). Treatment with HF and selective etching enable a more continuous, homogeneous, and regular distribution of diatom shells, with no or minimum contaminants in the samples (Fig. 1b). Resulting shells have a circular, hollow, cylindrical shape, with a mean diameter at the base of about a~5 μm and height of about b~10 μm (Fig. 1c). Regular, periodic arrays of pores permeate the surface of the diatoms penetrating through the shell (Fig. 2a–c). Image analysis algorithms applied to SEM images enable to derive the mean pore size as s~90 ± 5 nm. Pore size is distributed in narrow intervals with small deviations around the mean. Worthy of note, pores on the surface of the diatom are arranged following hexagonal patterns (Fig. 2c), similarly to the topology of photonic crystals, where periodic
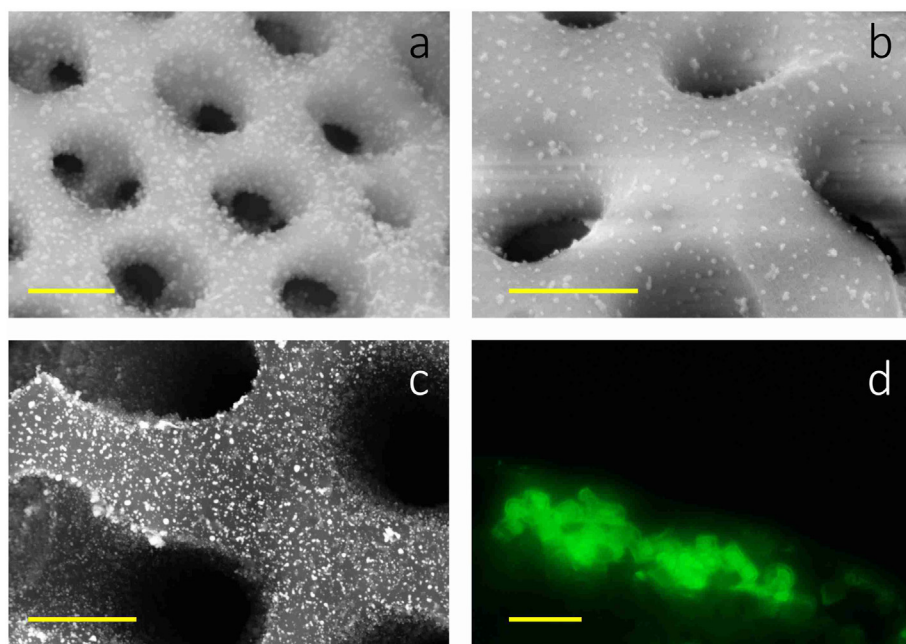

Fig. 3. Upon functionalization, gold nanoparticles are deposited on the external diatom surface and within the pores with an average nanoparticle size of 8 nm (a, b, c). Diatom shells functionalized with gold nanoparticles (D24 devices) were incubated with 50 nm Yellow fluorescent beads, fluorescent confocal imaging demonstrates selectivity and metal enhanced fluorescence of the D24 devices, scale bar in the image is 50 μm (d).

optical structures can control the flow of light, force light around sharp bands and manipulate the electromagnetic radiation in a designed fashion. This suggests that the characteristic internal structure of diatoms can serve as a basis for sensor devices with elevated precision and sensitivity.

We then used chemical methods and photo-deposition techniques (Methods) to functionalize the surface of diatoms with Au NPs. By changing the proportion of reactants in solution and the duration of the exposure to the external radiation, we obtained Au NPs with controlled size and density. A treatment of 1 h yields particles uniformly distributed over the entire surface of the diatoms and within the pores with an average particle size of $d = 8 \pm 4$ nm (Fig. 3a–c). We determined particle size distribution and average particle size through SEM image analysis. We call similar diatom shells functionalized with Au NPs, D24 devices.

While 8 nm does not represent the theoretical optimal size for detection and electromagnetic amplification, it is the best compromise between small nano-particles synthesis times and high enhancement factors during the generation of the Raman signal, as evidenced by experiments and computer simulations. For the present configuration,

the particles in the system are isolated: the enhancement factor of the device may be incremented even further if one fabricates gold nanoparticles combined in clusters, where interaction between particles may yield collective phenomena with improved abilities in contrast to isolated particles.

D24 devices have an internal intricate structure of pores that may be used to harvest and capture molecules in solution, and an external decoration of nanoparticles that can multiply the intensity of an electromagnetic (EM) radiation of several orders of magnitude. Upon incubation with yellow fluorescent nano-spheres and washing (Methods), fluorescent confocal imaging of the devices (Fig. 3d) demonstrates selective sequestration of the spheres, long-term retention, and metal enhanced fluorescence (MEF) effects, with an increased signal of fluorescence ascribed to the resonant interaction of the laser with the metal nano-particles of the diatoms [17]. We have used untreated diatom skeletons without gold nanoparticles as a negative control. Using simple diatom shells, we measured yellow fluorescent nano-beads in the same abundance ranges and setting the same parameters used for measuring fluorescence with the D24 devices. Results, reported in separate Supporting information file, show that diatoms without gold
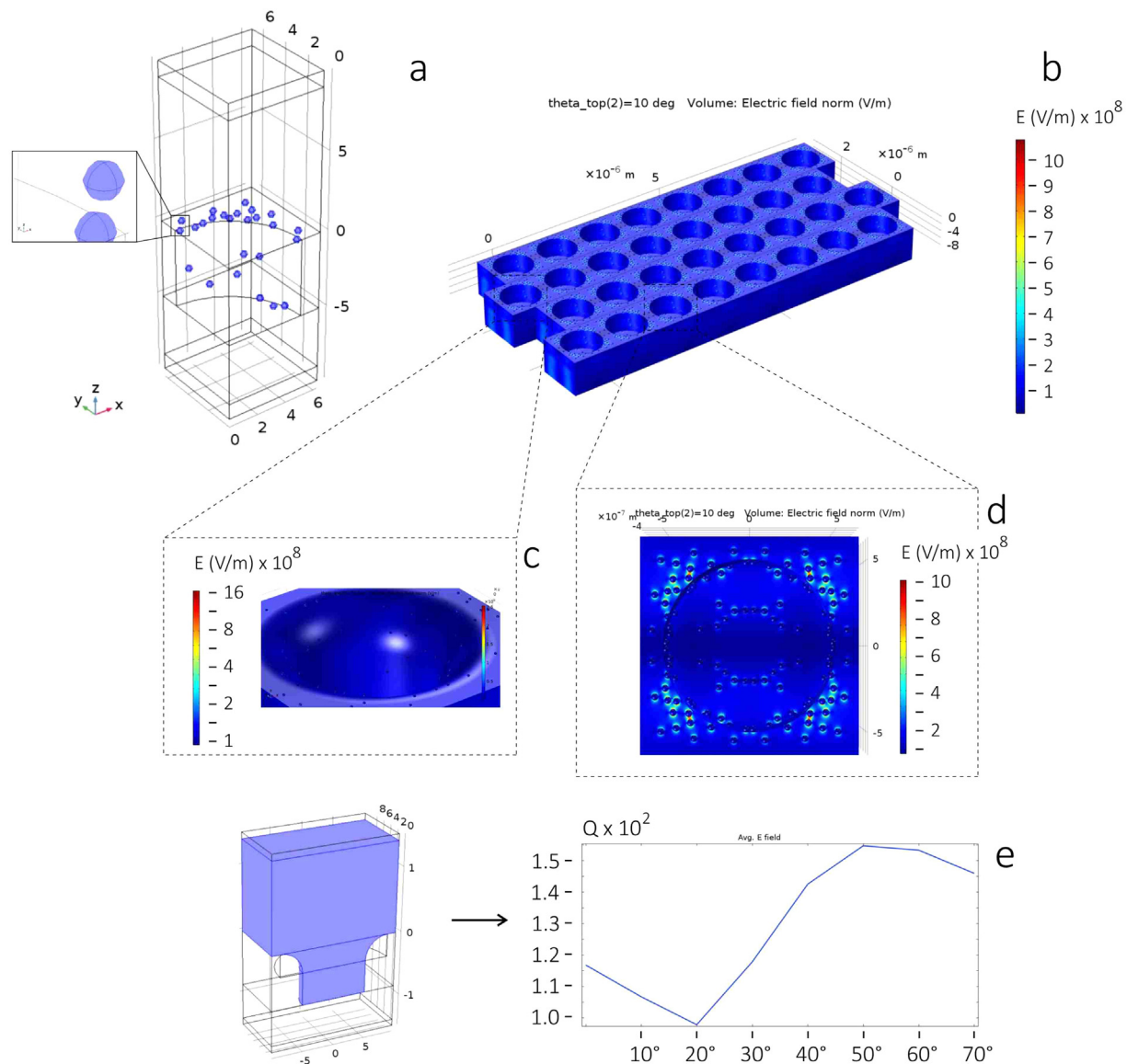

Fig. 4. We used finite element methods (FEM) to evaluate the distribution of the electromagnetic (EM) field around the clusters of gold nanoparticles and within the pores of the diatoms (a). Results indicate that the EM field is concentrated in close proximity of the particles (b). Maximum strength of the field is a function of the inclination α of the radiation that illuminates the system and may be as high as 1.5×10^9 V/m (c, d). The enhancement factor of the electric field oscillates between $Q\sim100$ and $Q\sim150$ for values of α varying between 10° and 70° (e).

nanoparticles yield a reduced intensity of fluorescence with respect to the D24 devices. Using image analysis algorithms, we estimate an enhancement of the fluorescent signal of approximately 80 times, moving from simple to functionalized diatom shells.

Computer simulations were used to evaluate the EM distribution around the nanoparticles and within the pores of the diatoms (Methods). Diatom frustule pores and gold nano-particles were reproduced in a grid, exploiting the symmetry of the system to reduce computation times, reduce memory usage, and increase the speed of the simulations (Fig. 4a). Then, results of the simulations have been periodically extended to visualize the diatom array (Fig. 4b). Results indicate that the EM field is greatly amplified in close proximity of the gold nano-particles and gold nano-particles clusters. Maximum intensity of the EM field is a function of the inclination α of the initial radiation with respect to the axis of the pore and may reach values as high as 1.6×10^9 V/m for $\alpha = 50°$ (Fig. 4c–d). The enhancement factor Q of the EM field is likewise a function of α (Fig. 4e) and is higher for higher values of α ranging between Q~115 ($\alpha = 30°$) and Q~170 ($\alpha > 50°$). Q > 10^2 for all configurations, yielding giant SERS (surface enhanced Raman Spectroscopy) amplification factors $Q_{Raman} = Q_{EM}^4$~10^8.

D24 devices were demonstrated for the detection and analysis of Bovine Serum Albumin (BSA) and mineral oil (MO) in extremely low abundance ranges. BSA is a globular protein used in numerous biochemical applications due to its stability and lack of interference within

biological reactions [18]. MO is a contaminant resulting from the distillation of petroleum used in manufacturing, food industry, cosmetic industry, and – for safety concerns – it is recommended to limit the exposition to MO in concentrations below 50 ppm [19]. Therefore, detecting BSA and MO is of interest in biology, biotechnology, biomedical engineering, environment, health and safety.

We incubated 1 mg of D24 devices in 1 ml of diluted BSA solution. We then separated the micro-capsules from the solution through sedimentation and used micro-Raman to examine the samples (Methods). We acquired Raman spectra of (i) the D24 devices without BSA, of (ii) BSA and of (iii) BSA internalized within the capsules. Results indicate (Fig. 5a) that D24 systems correctly detect the aromatic components of BSA at $f = 1392$ cm^{-1}, $f = 1556$ cm^{-1} and $f = 1576$ cm^{-1}, and Amide I at $f = 1670$ cm^{-1}, suggesting a $\beta-$ sheet conformation of the protein. BSA is observable in concentrations down to $c = 10^{-16}$ M.

Using the same methods, we examined MO in concentration varying from 50 to 10^5 ppm. In the spectra, the peak at $f = 950$ cm^{-1} is associated to the second-order scattering of Silicon [20], the peak at $f = 1450$ cm^{-1} identifies the CH$_2$ scissors vibration, the peaks in the $2850 - 2923$ cm^{-1} interval indicates CH stretching [21]. D24 systems can identify MO at extremely low abundance ranges of 50 ppm (Fig. 5b).

Although this test campaign was not focused on optimizing performance and was more an exercise in existence proof, still we tested the performance of the device with multiple measurements. The analysis
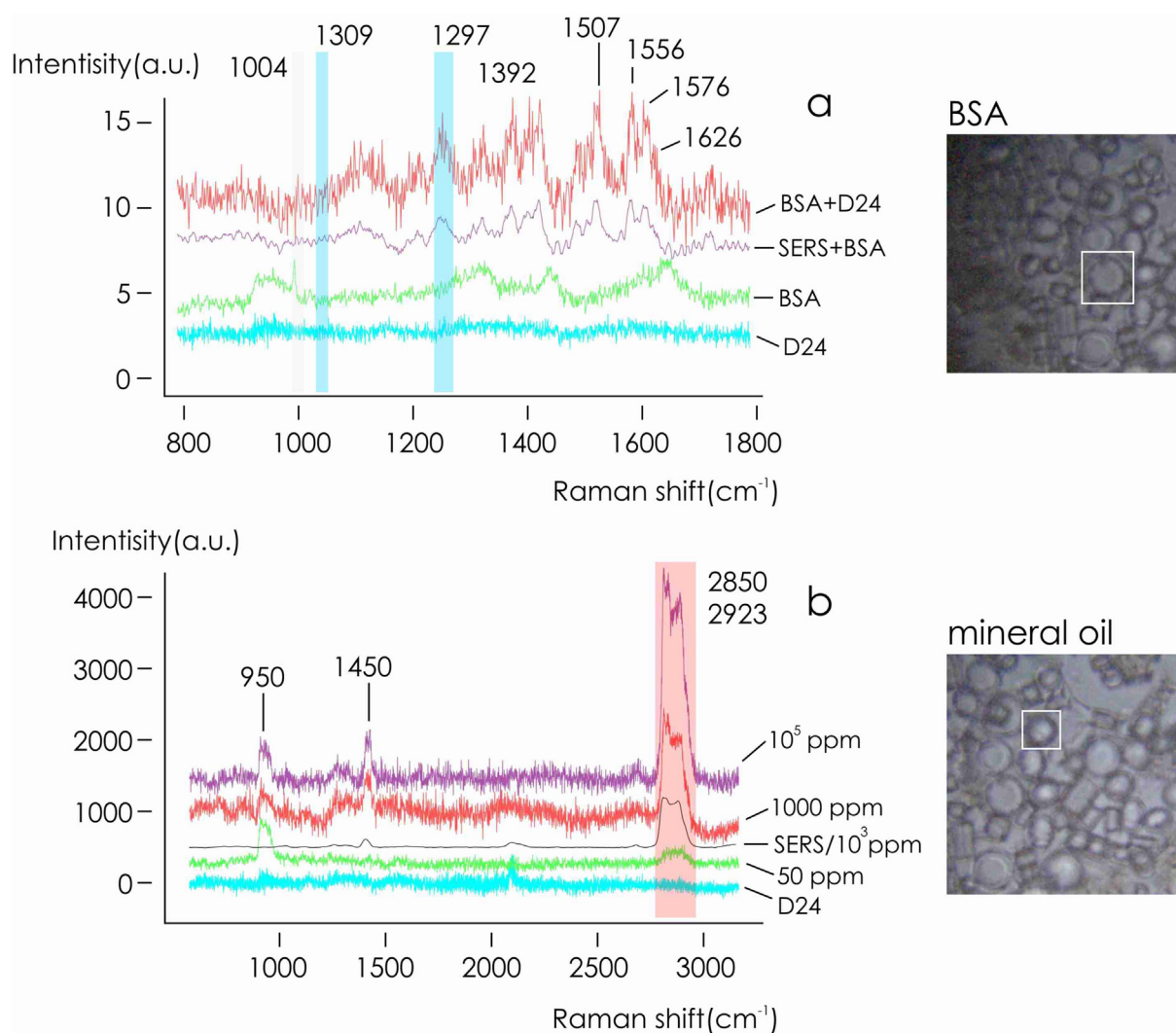

Fig. 5. The devices were verified for the analysis of Bovine Serum Albumin (BSA) (a) and mineral oil (mo) (b) with Raman spectroscopy. We detected BSA in solution with a concentration as low as $c = 10^{-16}M$, and mo with a concentration of 50 ppm.

was performed over 10 experimental repeats for BSA and MO, with 5 technical repeats for experiment. In the paper, we report sample spectra extracted from the pool of spectra. We observed that the variation intra-cluster (between technical repeats conducted over the same sample) is vanishingly low, with values of standard deviation lower than the 0.1% of the mean of measured spectra, the variation inter-cluster (between experimental repeats conducted over different samples) is higher, with values of standard deviation equal to about the 5% of the mean of measured spectra. Possibly because different samples, under different conditions, may contain different amounts of molecules, reflected by a variability of the measured spectra.

In Fig. 5, we have reported spectra acquired on standard SERS substrates for comparison. We observe that the analytes, measured on flat SERS substrates in higher concentrations, exhibit Raman profiles similar to those measured using the D24 device, with same characteristic Raman shifts, peaks, and spectral features. Comparison between measurements indicates that the precision and sensitivity of the D24 device is equivalent or superior of those of traditional SERS substrates.

D24 devices are intended for analyte capture, concentration, and detection. While concentrating the solute is important, it is not the main objective of the device. More importantly than concentrating, the device can sequestrate selectively analytes from a solution. Upon incubation in a solution, for its geometrical characteristics the diatoms would harvest the molecules of interest dispersed in that solution – that are otherwise hardly accessible. Then, one may collect the devices with their payload using sedimentation, centrifugation, or other separation techniques routinely used in a laboratory. Upon recovery, the devices are then ready for high end, precise measurement of the solute initially dispersed in solution. The major attribute of the device is a combination of factors, it achieves high resolution, it is practical and enables analyte capture and handling, it is low cost. The last characteristic, in turn, allows one to use the device in high-throughput screening and processes, where the number of devices deployed for the analysis may be very large.

In more sophisticated evolutions of the device that will be developed over time, one shall be able to selectively capture molecules of arbitrary dimension in solution by tuning pore size. In the case of a mixture of different oils, the penetration depth ζ of a specific oil in the system can be estimated using the Jurin's law: $\zeta = 2\,\gamma\,cos\vartheta / \varrho\,g\,s$, where γ is the surface tension of the oil, ϱ is its density, s is the pore size of the device, g is the gravitational acceleration, ϑ is the angle of contact between the diatom surface and the oil. Competition between gravitational and capillary forces determines the fraction of oil that the system can adsorb. Thus, by tuning the pore size s, one can selectively sequestrate and measure specific oils with specific physical characteristics γ, ϱ, ϑ, from the mixture. Similarly in concept to a molecular filter, but extended to solutions and mixtures in which both the solvent and the solute are liquids.

4. Conclusions

We conceived chemical methods to purify and functionalize inhomogeneous, unpurified diatomaceous earth and obtain miniaturized devices where the porous structure of the devices can harvest analytes from a solution, and the gold nano-particles infiltrated through the pores amplify the EM radiation of several orders of magnitude. The combination of these effects enables the analysis of biological molecules, chemical analytes, or pollutants in aqueous solutions in heretofore unattainable abundance ranges. In experiments with BSA, we detected proteins in solution with a concentration of 100 *aM*. In experiments with mineral oil, we detected contaminants in solution down to 50 *ppm*. Our method can turn an unlimited, low cost, natural material into efficient sensing devices for applications in biology, marine biology, biotechnology, safety, monitoring and control of environmental hazards.

Conflicts of interest

The authors declare no conflict of interest.

Data availability

Data presented in the MS are available upon request.

Appendix A. Supplementary data

Supplementary data to this article can be found online at https://doi.org/10.1016/j.mne.2018.11.006.

References

[1] J. Bradbury, Nature's nanotechnologists: unveiling the secrets of diatoms, PLoS Biol. 2 (2004) e306.

[2] M. Mishra, A.P. Arukha, T. Bashir, D. Yadav, G.B.K.S. Prasad, All new faces of diatoms: potential source of nanomaterials and beyond, Front. Microbiol. 8 (2017).

[3] Z.H. Aitkena, S. Luob, S.N. Reynoldsc, C. Thaulowd, J.R. Greerb, Microstructure provides insights into evolutionary design and resilience of *Coscinodiscus* sp. Frustule, Proc. Natl. Acad. Sci. U. S. A. 113 (2016) 2017–2022.

[4] M.A. Ferrara, P. Dardano, L. De Stefano, I. Rea, G. Coppola, I. Rendina, R. Congestri, A. Antonucci, M. De Stefano, E. De Tommasi, Optical properties of diatom nanostructured biosilica in *Arachnoidiscus* sp: micro-optics from mother nature, PLoS One 9 (2014) (e103750-103751-103758).

[5] J. Romann, J.-C. Valmalette, M.S. Chauton, G. Tranell, M.-A. Einarsrud, O. Vadstein, Wavelength and orientation dependent capture of light by diatom frustule nanostructures, Sci. Rep. 5 (2015) 1–6.

[6] J. Romann, J.-C. Valmalette, A. Røyset, M.-A. Einarsrud, Optical properties of single diatom frustules revealed by confocal microspectroscopy, Opt. Lett. 40 (2015) 740–743.

[7] S. Yamanaka, R. Yano, H. Usami, N. Hayashida, M. Ohguchi, H. Takeda, K. Yoshino, Optical properties of diatom silica frustule with special reference to blue light, J. Appl. Phys. (2008) 103.

[8] I. Rea, M. Terracciano, S. Chandrasekaran, N.H. Voelcker, P. Dardano, N.M. Martucci, A. Lamberti, L. De Stefano, Bioengineered silicon diatoms: adding photonic features to a nanostructured semiconductive material for biomolecular sensing, Nanoscale Res. Lett. (2016) 11.

[9] K.H. Sandhage, M.B. Dickerson, P.M. Huseman, M.A. Caranna, J.D. Clifton, T.A. Bull, T.J. Heibel, W.R. Overton, M.E.A. Schoenwaelder, Novel, bioclastic route to self-assembled, 3D, chemically tailored meso/nanostructures: shape-preserving reactive conversion of biosilica (diatom) microshells, Adv. Mater. 14 (2002) 429–433.

[10] J.Q. Dalagan, E.P. Enriquez, L.-J. Li, C.-T. Lin, Growth of copper on diatom silica by electroless deposition technique, Mater. Sci.-Pol. 31 (2013) 226–231.

[11] M. Pannico, I. Rea, S. Chandrasekaran, P. Musto, N.H. Voelcker, L. De Stefano, Electroless gold-modified diatoms as surface-enhanced Raman scattering supports, Nanoscale Res. Lett. (2016) 11.

[12] G. Bertoni, F. Fabbri, M. Villani, L. Lazzarini, S. Turner, G. Van Ten-deloo, D. Calestani, S. Gradečak, A. Zappettini, G. Salviati, Nanoscale mapping of plasmon and exciton in ZnO tetrapods coupled with Au nanoparticles, Sci. Rep. 6 (2016) 1–8.

[13] S. Picciolini, N. Castagnetti, R. Vanna, D. Mehn, M. Bedoni, F. Gramatica, M. Villani, D. Calestani, M. Pavesi, L. Lazzarini, A. Zappettini, C. Morasso, S. Picciolini, N. Castagnetti, R. Vanna, D. Mehn, M. Bedoni, F. Gramatica, M. Villani, D. Calestani, M. Pavesi, L. Lazzarini, A. Zappettini, C. Morasso, Branched gold nanoparticles on ZnO 3D archi-tecture as biomedical SERS sensors, RSC Advances, 5 (2015) 93644–93651 RSC Advances,.

[14] M.L. Coluccio, F. Gentile, M. Francardi, G. Perozziello, N. Malara, P. Candeloro, E. Di Fabrizio, Electroless deposition and nanolithography can control the formation of materials at the nano-scale for plasmonic applications, Sensors 14 (2014) 6056–6083.

[15] F. Gentile, M. Coluccio, A. Toma, E. Rondanina, M. Leoncini, F. De Angelis, G. Das, C. Dorigoni, P. Candeloro, E. Di Fabrizio, Electroless deposition dynamics of silver nanoparticles clusters: a diffusion limited aggregation (DLA) approach, Microelectronic Eng. 98 (2012) 359–362.

[16] A.D. Rakic, A.B. Djurisic, J.M. Elazar, M.L. Majewski, Optical properties of metallic films for vertical-cavity optoelectronic devices, Appl. Opt. 37 (1998) 5271–5283.

[17] E. Battista, M.-L. Coluccio, A. Alabastri, M. Barberio, F. Causa, P.-A. Netti, E. Di Fabrizio, F. Gentile, Metal enhanced fluorescence on super-hydrophobic clusters of gold nanoparticles, Microelectron. Eng. 175 (2017) 7–11.

[18] F. Gentile, M.L. Coluccio, R.P. Zaccaria, M. Francardi, G. Cojoc, G. Perozziello, R. Raimondo, P. Candeloroa, E.D. Fabrizio, Selective on site separation and detection of molecules in diluted solutions with superhydrophobic clusters of plasmonic nanoparticles, Nanoscale 6 (2014) 8208–8225.

[19] K. Grob, Could the Ukrainian sunflower oil contaminated with mineral oil wake up sleeping dogs? Eur. J. Lipid Sci. Technol. 110 (2008) 979–981.

[20] D. Lin-Vien, N. Colthup, W. Fateley, J. Grasselli, The Handbook of Infrared and Raman Characteristic Frequencies of Organic Molecules, Academic Press, 1991.

[21] D. Orange, E. Knittle, D. Farber, Q. Williams, Raman spectroscopy of crude oils and hydrocarbon fluid inclusions: a feasibility study, International Mineralogical Association: mineral spectroscopy; a tribute to Roger G, Burns 5 (1996) 65–82.